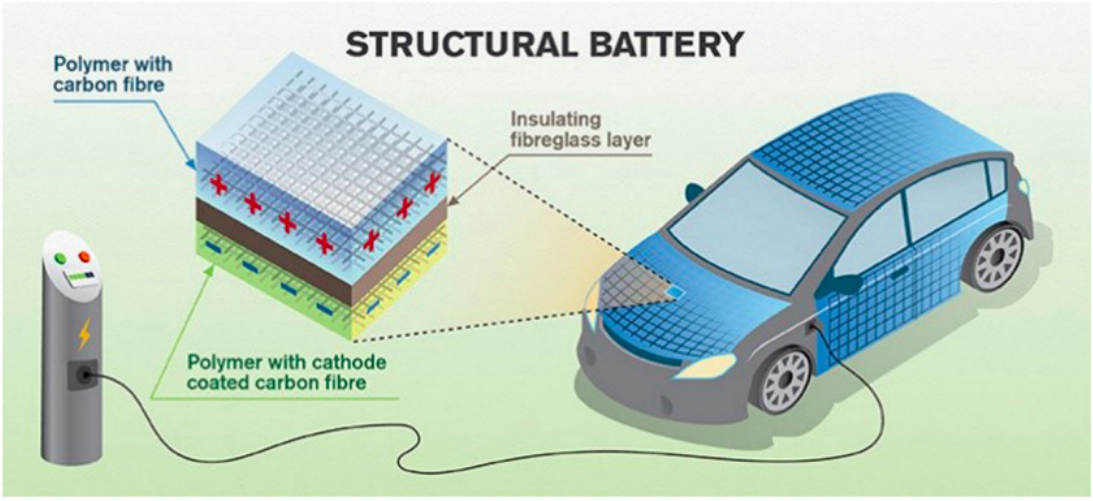

Coupled Multi-Physical Processes in Structural Battery Composites

Master's thesis in Applied Mechanics

CLARA DAHLBERG

DEPARTMENT OF INDUSTRIAL AND MATERIALS SCIENCE

CHALMERS UNIVERSITY OF TECHNOLOGY
Gothenburg, Sweden 2023
www.chalmers.se

Master's thesis 2023

Coupled Multi-Physical Processes in Structural Battery Composites

Clara Dahlberg

CHALMERS
UNIVERSITY OF TECHNOLOGY

Department of Industrial and Materials Science
Division of Material and Computational Mechanics
Chalmers University of Technology
Gothenburg, Sweden 2023

Coupled Multi-Physical Processes in Structural Battery Composites
Clara Dahlberg

Supervisor: Johanna Xu, Industrial and Materials Science
Examiner: Leif Asp, Industrial and Materials Science

Master's Thesis 2023
Department of Industrial and Materials Science
Division of Material and Computational Mechanics
Chalmers University of Technology
SE-412 96 Gothenburg
Telephone +46 31 772 1000

Cover: Schematic view of electricity storage in a car. Image by Yen Strandqvist, Chalmers University of Technology

Typeset in LaTeX
Printed by Chalmers Reproservice
Gothenburg, Sweden 2023

Coupled Multi-Physical Processes in Structural Battery Composites
Clara Dahlberg

Department of Industrial and Materials Science
Chalmers University of Technology

Abstract

This thesis examines the change in open cell potential when a structural battery, at a constant state of charge, is exposed to a tensile load.
A structural battery full-cell was manufactured. It was electrochemical cycled before being clamped into a tensile machine. In the tensile machine, a potentiostat was connected to the cell which measured the Open Circuit Potential (OCP) while the cell was exposed to a varying tensile load. Two of the three cells used during the experiment were fully delithiated and the third was fully lithiated. The coupling factor was also calculated to gain an understanding of how the cell was affected by different states of charge and different loads.
The results show that when the load increases, the cell potential decreases, but when the load decreases, the potential increases. This response is immediate for all three cells and the response of the potential is not strain rate dependent. The state of charge shows that a fully lithiated cell has a lower coupling factor than a fully delithiated cell. This is in accordance with previous experiments in the open literature performed on the half-cell as the cell shows a similar behavior, but the coupling factor is higher for the delithiated cell than for the lithiated cell.
The conclusion that can be drawn after performed experiments is that the model used works to validate and investigate the behavior of the coupling factor in the full-cell under different states of charge and varying tensile loads.

Keywords: Structural Batteries, Composites, Carbon fiber, Piezo-electrochemical effect.

Acknowledgements

I would like to thank my supervisor Johanna Xu for all her help with the experiments, the report and for answering all my thousand and one questions during the course of the work. Without your help I would not have been able to submit a work that I am very happy with. Thank you for helping me brainstorm ideas for both the experiments, the report and the presentation.

I would also like to thank my examiner Leif Asp for his dedication and cheerful encouragement during the work, you made me more interested in structural batteries than I ever thought was possible.

Thanks to Emelie Seignér for your help in the lab, your company and for proofreading my report and presentation.

A big thank you to everyone in the department who asked how things are going, showed interest in my work, answered questions and showed support during the past months. Thanks for all the fun coffee breaks and interesting lunch discussions.

Clara Dahlberg, Gothenburg, June 2023

Contents

List of Figures

List of Tables

Acronyms

BPAMA Bishpenol A Ethoxylate Dimethacrylate. 10

Deben Deben Microtest. 11

EC Ethylene Carbonate. 10

Gamry Gamry Instruments Framework. 11

LFP Lithium-Iron-Phosphate. 5, 9, 10, 19, 20
Li Lithium. 5
Li-ion Lithium-ion. xi, 1, 2, 17
LiBoB Lithium Bis(oxalato)borate. 10
LiTf Lithium Triflouromethanesulfonate. 10

OCP Open Circuit Potential. v, 11, 19, 20

PC Propylene Carbonate. 10

SBE Structural Battery Electrolyte. 3, 6, 10, 17, 19, 20, 23
SOC State of Charge. 14, 18–21, 23

1
Introduction

One of the most common battery type is the Lithium-ion (Li-ion) battery. Some applications that are powered by a Li-ion battery are small electronic devices, such as laptops and smartphones, and vehicles among other things. A great disadvantage with today's batteries is that they add weight to the system. Considering a Tesla model 3 with a battery weight of 490 kg, which is approximately 27 % of the vehicle's total weight [1]. A heavier car needs more power to drive, thereby a larger battery is needed, which creates a circle of demands. If the range of today's electric vehicles is to increase, the batteries must have larger capacity and therefore be larger, resulting in a significantly heavier vehicle. Heavy vehicles consume more energy. To realize more energy-efficient vehicles, mass must be reduced. This is where multi-functional structural batteries can play a major role. By developing a battery with a load carrying capability and slightly reduced capacity compared to today's batteries, the battery can be integrated in the vehicle structure, e.g. the body-in-white [2]. With such an integrated structural battery, as seen in figure 1.1, the total weight of, for example, electric vehicles could be significantly reduced [3].

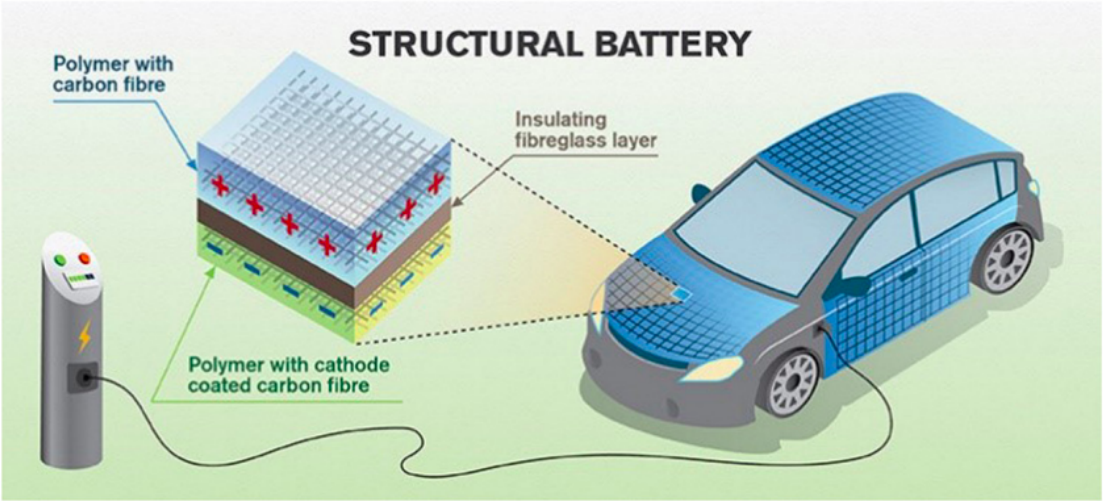

Figure 1.1: Schematic view of electricity storage in a car [4].

1.1 Background

A Li-ion battery is an electrochemical device that convert chemical energy to electrical energy, it consists of a positive electrode and a negative electrode, electrolyte, current collectors and a separator, as illustrated in figure 1.2. When the battery is charged, the Li-ions flows from the positive electrode to the negative electrode creating an electrical current that charges the device. When the battery is discharged, the Li-ions flows in the opposite direction and the stored electrical energy can be used to perform external work, e.g. propelling the vehicle [5].

In a conventional Li-ion battery, the negative electrode consists of a graphite mix, which in some cases can contain up to 5% silicon to increase the energy density. The positive electrode consists of different materials depending on desired battery properties. Common materials used are metal oxides, such as lithium-cobalt oxide and lithium-nickel-cobalt-aluminum oxide, alternatively iron phosphate, such as lithium-iron phosphate.

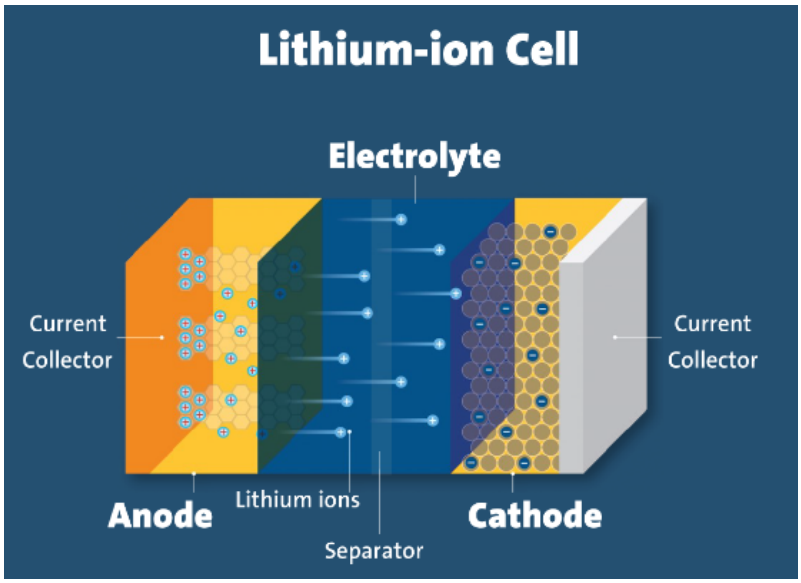

Figure 1.2: Schematic view of a Li-ion battery [5].

Structural batteries are multifunctional devices that simultaneously store energy and bear mechanical loads. Li-ion battery is utilized, with carbon fiber playing a crucial role as both structural reinforcement and an electrode capable of reversibly hosting Li-ions.

It is important to distinguish between two different concepts of structural batteries. One is to insert a thin battery inside the sandwich structure of a composite material. This multifunctional component is then made from two monofunctional devices [6–8]. The second concept is to manufacture a composite material with multiple intrinsic functionalities, for example a material that can sustain both mechanical loads while storing electrochemical energy as a battery [6, 9].

For the multifunctional material, two different designs of structural batteries have been researched. The first design is a laminated device, in which a lamina constitutes a structural negative electrode and another lamina the structural positive electrode, separated by an electrically insulating separator layer [2, 10]. The entire laminate is impregnated with a Structural Battery Electrolyte (SBE). The second design of structural battery composites is the so-called micro-battery material that uses a unidirectional array of individually polymer electrolyte-coated carbon fibers in a cathode-doped polymer matrix [11–13]. Recently, a research team has also presented a structural micro-battery that has been manufactured using a 3D-printing technique [12, 13].

A laminated structural battery with reasonable modulus of elasticity and electrical energy density has recently been fabricated. No battery before had been developed that combined both good mechanical and electrochemical properties. Previous works have only reported data for stiffness and strength in the fiber direction and not in the direction perpendicular to the fibers [2].

The current study concerns the latter concept, i.e., the multifunctional material with an intrinsic capability to work as a structural battery. AS such, the study concerns the laminated device.

1.2 Aim

The project aims to develop methods for the characterization of laminated structural batteries under combined electrochemical and mechanical loads. These methods and their results will be used for the validation and further development of a multiphysics computational framework.

1.2.1 Goal

- Determine to what extent the potential of the battery changes when a constant current and a varying mechanical load is applied.

2
Theory

This section serves to introduce the key topics used throughout this report. First, a brief introduction to a structural battery is presented, as well as a description of carbon fiber and its properties. Finally, a presentation of what the Piezo-electrochemical effect is described.

2.1 Structural Battery

There are two types of structural batteries reported in the literature, the full-cell and the half-cell, both are electrochemical cells but made up of different materials. The full-cell consists of carbon fiber and a Lithium-Iron-Phosphate (LFP) foil, while the half-cell consists of carbon fiber and Lithium (Li) metal foil. Both cells are immersed in an electrolyte. The material with the higher standard electrode potential acts as the positive electrode of the structural battery and the lower one as the negative electrode. For the full-cell, the LFP foil has a higher standard electrode potential than the carbon fiber and therefore acts as the positive electrode and the carbon fiber as the negative. Compared to the half-cell where the carbon fiber has the higher standard electrode potential than the Li metal and therefore acts as the positive electrode and the Li metal as the negative. During cycling (lithiation and delithiation) the following reactions occurs in the full-cell:

$$LiFePO_4 + 6C \leftrightarrow FePO_4 + LiC_6 \tag{2.1}$$

and for the half-cell the following reactions occurs:

$$Li_x + C_6 \leftrightarrow C_6Li_x \tag{2.2}$$

where x is the unknown parameter which depends on the chemical composition of carbon fiber [14].

The difference between the potentials of the positive and negative electrodes is called the cell potential. The change in potential during lithiation and delithiation depends on the concentration of lithium ions inserted into the fibers.

The specific electrochemical capacity of a cell reflects the amount of lithium ions inserted in the carbon fibers and is calculated with the following equation:

$$C_s^{measured} = \int Idt/m \tag{2.3}$$

where I is the constant current used to cycle the cell, $\int Idt$ is the definite integral of the measured current over the the lithium-intercalation reaction duration and m the mass of the carbon fiber electrode. The capacity measured for a lithiation is defined as the amount of electric charges received by the cell for the duration of the lithiation normalized by the mass of the carbon fiber.

The SBE is the component that provides mechanical integrity to the structural battery. It determines much of the mechanical and electrochemical performance of the cell. There are two phases in the electrolyte, the solid polymer phase and the liquid electrolyte phase, see figure 2.1. The liquid phase of the SBE has a high ionic conductivity but no structural properties, while the solid phase has high mechanical stiffness and strength but no ion conductivity. Since the relationship between the mechanical strength and the ionic conductivity is inverse, see figure 2.2, it is difficult to produce an electrolyte possessing both these properties [15].

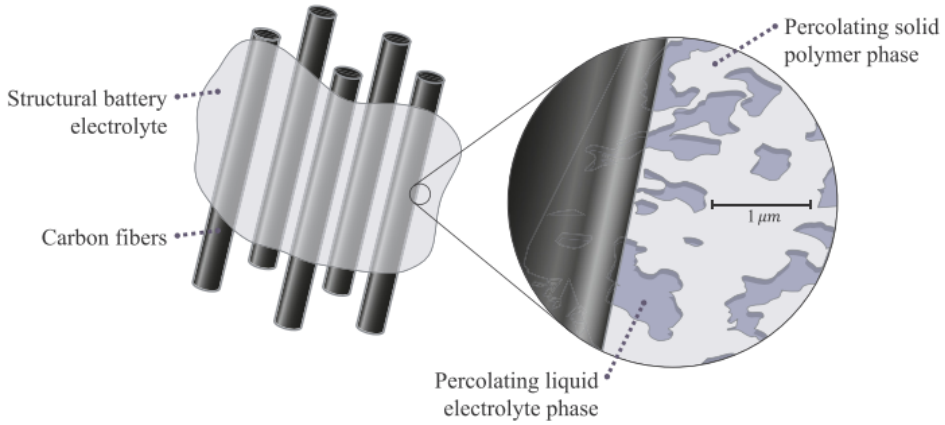

Figure 2.1: Schematic of carbon fibers in a structural battery electrolyte [16].

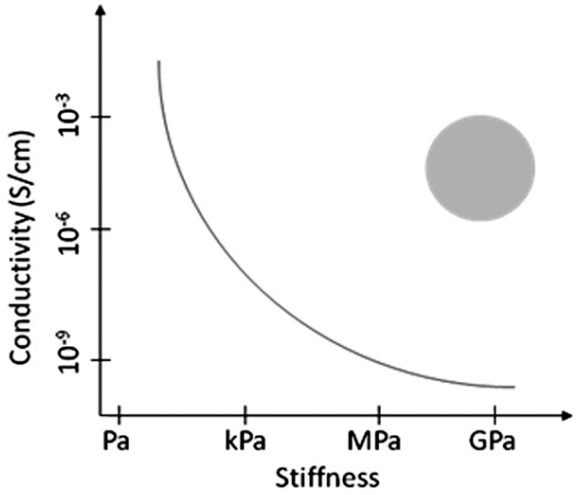

Figure 2.2: Schematic of lithium ion conductivity versus stiffness for solid polymer electrolytes [17].

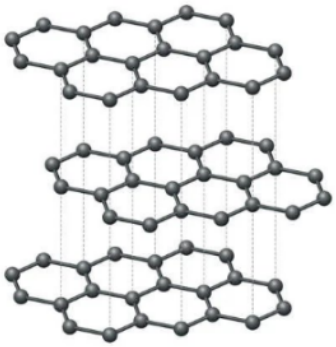

(a) Graphite structure [20].

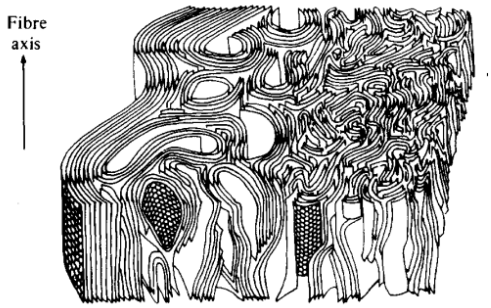

(b) Turbostratic graphite structure [21].

Figure 2.3: The schematic view of the carbon fiber structure at an anatomical level.

2.2 Carbon Fiber

Carbon fiber dates back to the latter half of the 19th century where it was used in incandescent light bulbs. The material is made out of strong, thin crystalline layers of carbon filaments where the fibers are about 5 to 10 micrometers in diameter, measuring thinner than a strand of human hair. Each layer has a hexagonal form, see figure 2.3a, and the interlayer spacing is approximately 3.4 Å. The turbostratic graphite structure of carbon fiber can be seen in figure 2.3b. Other beneficial properties of carbon fiber are its high tensile strength and high Young's modulus, ranging between 2 and 7 GPa and 200 and 600 GPa, respectively [18]. Due to the strong parallel alignment of the graphene planes in the fiber direction, the longitudinal modulus is significantly higher than the radial modulus [19].

Carbon fibers are used in structural batteries as electrodes since it enables the battery to carry mechanical loads. When employing the carbon fiber as a electrode the structural battery can have longitudinal modulus (modulus in the fiber direction) of 117 GPa. In comparison with the commercial graphite crystal, the carbon fiber has an elastic modulus around 30 times higher, even though the interlayer spacing between the layers is greater, 3.35 Å and 3.4 Å, respectively [19].

2.2.1 Lithiated Carbon Fiber

A lithiated carbon fiber is a carbon fiber with lithium in its microstructure. A recent study showed that the elastic modulus in the transverse direction increased from 7.5 GPa to 15.3 GPa, and decreased from 290 GPa to 255 GPa in the longitudinal direction when the carbon fiber has been lithiated. When the carbon fiber was delithiated, the elastic modulus in the transverse direction went down to 7.6 GPa and retrieved 290 GPa in the longitudinal direction. According to the same study, the initial interlayer spacing of pristine carbon fiber was measured to 3.45 Å. The average interlayer spacing after the first lithiation expanded to 3.87 Å and an average cross-section area expansion of 13.7% was measured. After the delithiation of the

carbon fiber the average interlayer spacing was decreased to 3.72 Å [19].

2.2.2 Piezo-electrochemical effect

When certain solid materials are deformed, the mechanical work is converted into electricity, this phenomenon is called Piezo-electricity and was discovered in the late 19th century. The Piezo-electric effect is also reversible, meaning that the mechanical work done on a material is converted to electrical charge and when a material is subjected to an electrical change, it is converted to mechanical work. The effect results from the linear electromechanical interaction between the electrical and mechanical states in crystalline materials with no inversion symmetry. The Piezo-electric effect has been exploited in many useful applications, including the production and detection of sound among other things.

The main difference between the Piezo-electric effect and the Piezo-electrochemical effect is that the Piezo-electrochemical effect occurs when the material is lithiated. The Piezo-electrochemical effect is also called the voltage-strain coupling effect. Previous studies on the voltage-strain coupling effect have been done on the carbon fiber negative half-cells, but until now no similar studies have been reported for full-cells [22–24].

The coupling factor k is a numerical measure of the voltage-strain coupling effect and indicates the magnitude of the voltage change per unit strain. A higher coupling factor is favorable for strain sensing and energy harvesting applications as it allows more sensitive strain measurements to be obtained [23, 24].

The coupling factor k is defined as

$$k = \frac{\Delta E}{\Delta \varepsilon} \tag{2.4}$$

where ΔE is the change of potential in the cell and $\Delta \varepsilon$ is the variation of the axial tensile strain in the carbon fiber. The axial tensile strain was calculated as

$$\varepsilon = \frac{L - \Delta L}{L} \tag{2.5}$$

where L is the original length of the cell and ΔL is the extension of the cell.

3
Methods

This section describes the methods used to determine the change in potential of a structural battery subjected to a tensile load. The first part explains the manufacturing of a structural battery while the second part presents how the experiments were carried out and the last part explains how the coupling factor was calculated.

3.1 Construction and manufacturing of structural batteries

The manufacture of the batteries used in the experiments consisted of two main steps, the first was the structural battery cell preparation and the second was the manufacture of the structural battery itself. In the sections below, these two steps are described in detail.

3.1.1 Structural Battery cell preparation

The size of the structural batteries were to be determined in the initial state. The longest and shortest distance in the tensile machine was measured and length was chosen in between these two values which gave room for extension of the structural batteries. A template, displayed in figure 3.1, was created to more easily manufacture the structural batteries to the same length.

For the experiments carried out in this thesis, the electrodes of the structural battery were made of commercial carbon fiber and a LFP foil, where the carbon fiber acted as the negative electrode while the LFP foil acted as the positive electrode. The LFP foil measured approximately 50 mm long and 10 mm wide. The two electrodes were separated by a 70 mm long and 15 mm wide Whatman GF/A separator. The current collectors measured 70 mm long and 5 mm wide, and the materials that were used for the negative and the positive current collectors was copper and aluminum. At the far ends of the structural battery, 10x10 mm glass fiber composite tabs were placed and used to correctly transfer the load from the clamps in the tensile machine to the structural battery cell. A piece of epoxy adhesive, the same size as the tabs, was placed between each layer of the cell and a coat of silver conductive paint was used to attach the carbon fiber tow to the copper current collector.

When the cell was assembled according to figure 3.2, the carbon fibers and the

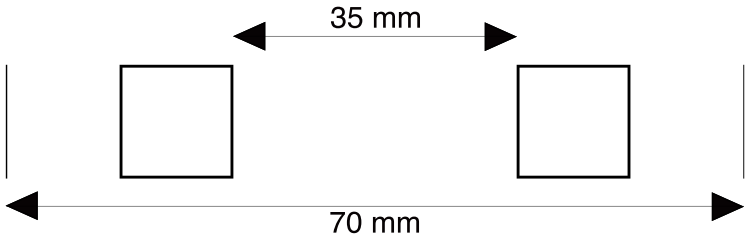

Figure 3.1: Template used during the structural battery cell preparations.

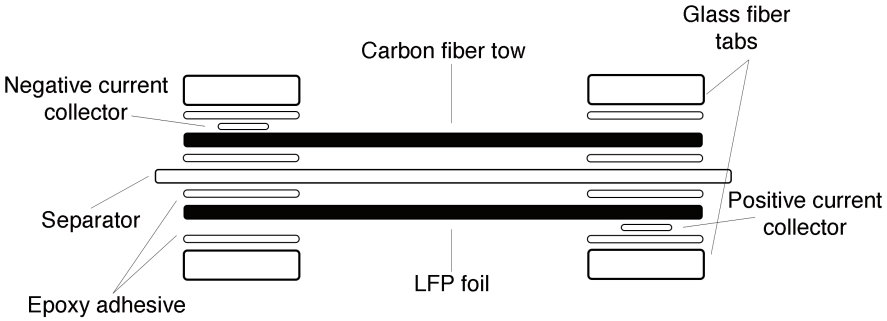

Figure 3.2: Schematic of cross-section of structural battery cell for expansion and voltage-strain coupling measurements.

LFP foil were slightly stretched to ensure fiber alignment. The cell was then placed in the oven for 1 hour at 90 °C under pressure to cure the epoxy adhesives.

3.1.2 Structural Battery manufacturing and battery cycling

The battery manufacturing was carried out in a glove box with inert argon atmosphere with less than 2 ppm O_2 and H_2O at ambient temperature.

The liquid electrolyte used in the SBE consisted of 6.5 g Ethylene Carbonate (EC), 6.5 g Propylene Carbonate (PC), 0.94 g Lithium Triflouromethanesulfonate (LiTf) and 0.78 g Lithium Bis(oxalato)borate (LiBoB). Equal parts monomer (Bishpenol A Ethoxylate Dimethacrylate (BPAMA)) and liquid electrolyte was mixed together, along with heat initiator corresponding to 1% of the total weight. This resulted in approximately 2.02 g of SBE that was dropped onto the cell after it was placed in an aluminum pouch bag.

The pouch bag was sealed at the same time as vacuum was drawn from the bag to ensure good contact between all layers and prevent evaporation of the SBE, and the cell was taken out of the glove box and placed in the oven for the electrolyte to cure under pressure at a temperature of 90 °C. After 1 hour, the cell was taken out and left to cool in room temperature, then plugged into the battery tester Neware CT-4008-5V10mA-164 for electrochemical cycling.

Each cycle contained four consecutive steps that were repeated five times. The first step was galvanostatic charging, where the cell was charged with a current of

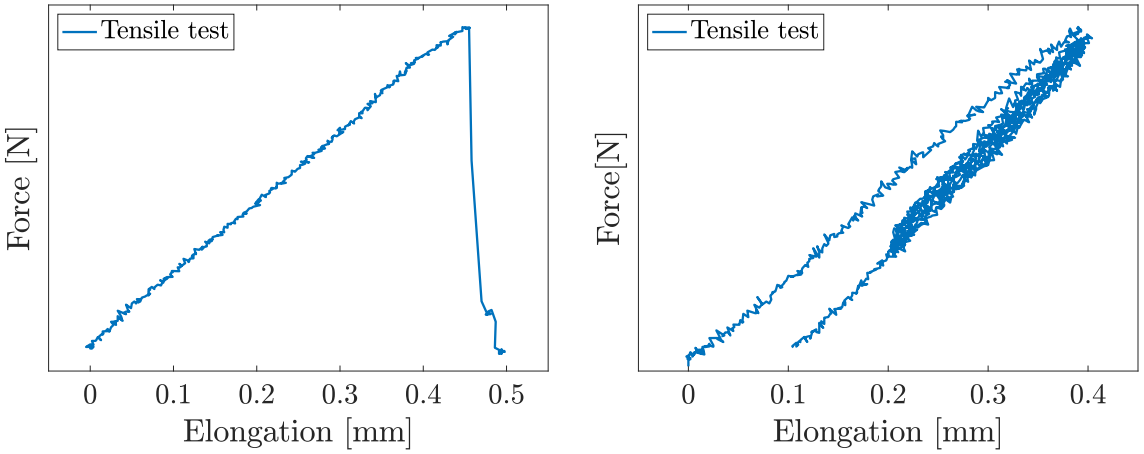

Figure 3.3: Tensile tests. a) cell stretched until breaking point. b) cell stretched to an elongation between 0.2 and 0.4mm.

0.0001 A until a voltage of 3.55 V was reached. The second step was an Open Circuit Potential (OCP) that allowed the cell to relax for 2 hours. The third step was galvanostatic discharge, where the cell was discharged with a current of 0.0001 A until a voltage of 2 V was reached. The fourth step was another OCP that allowed the cell to relax for 2 hours. When the cycle count was completed the cell was allowed to relax for 5 hours, before being removed.

3.2 Experiments

The experiments were carried out in a glove box with inert argon atmosphere with less than 2 ppm O_2 and H_2O at ambient temperature.

In order to establish how much tensile load the cell could take, experiments were first carried out where the cell was stretched to the breaking point at 0.45 mm corresponding to 1.3% strain, seen in figure 3.3, and two values below this point were then chosen. For the experiments performed in this thesis, the cell was stretched to an elongation of 0.2 and 0.4 mm. The elongations correspond to 0.6% and 1.1% strain, respectively.

3.2.1 Constant voltage and varying force

The cell was clamped in the tensile machine according to figure 3.4. During the experiment, the program Gamry Instruments Framework (Gamry) was used to measure the OCP of the cell and the program Deben Microtest (Deben) was used to control the tensile machine. The displacement rates used in Gamry were 0.2 mm/min and 0.5 mm/min, corresponding to a strain rates of $95 \cdot 10^{-6}$ s^{-1} and $24 \cdot 10^{-5}$ s^{-1}, respectively. The sample time was of 0.5 seconds and the entire program was set to run for between 1000 and 2500 seconds depending on the displacement rate and rest time set in Deben. In Deben, the program was set so that the tensile machine

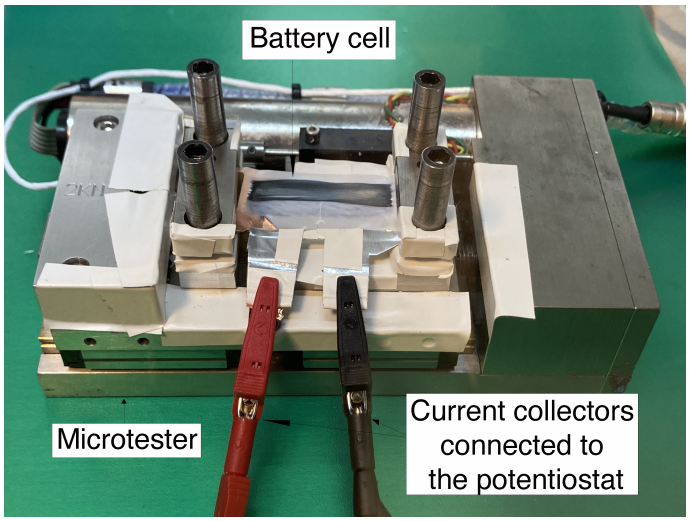

Figure 3.4: Attachment of the battery cell in the tensile machine with the current collectors connected to the potentiostat.

would run for five cycles, alternating between 0.6% and 1.1% strain, and the data sample time was 500 ms.

For each cell, two experiments were performed, one for each displacement rate.

3.3 Calculation of the coupling factor

The coupling factor was calculated using equation (2.4). Two time steps were chosen during the second cycle, the time steps would be either when the cell was loaded or unloaded. With the help of these time steps, the corresponding voltage and force could be obtained from figure 3.5.

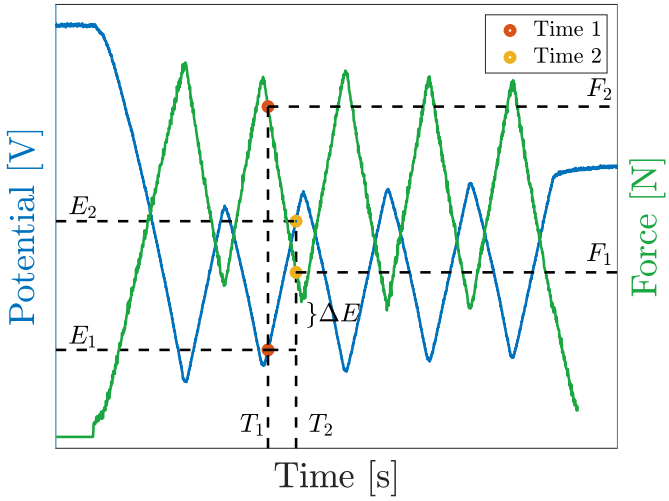

Figure 3.5: Determination of the variables used when calculating the coupling factor.

4
Results

Out of 24 made structural batteries only results from three were obtained, which are stated here. During the experiments, the carbon fibers in cell A and C were delithiated while cell B was lithiated.

4.1 Electrochemical cycling

Figure 4.1 shows the electrode potential during the first and the fifth electrochemical cycle. The first-cycle capacity is 8.91 mAh/g, dropping to 3.54 mAh/g for the fifth cycle when the carbon fibers in the cell is lithiated. The first-cycle discharge capacity is 4.05 mAh/g and drops to 3.03 mAh/g for the fifth cycle.

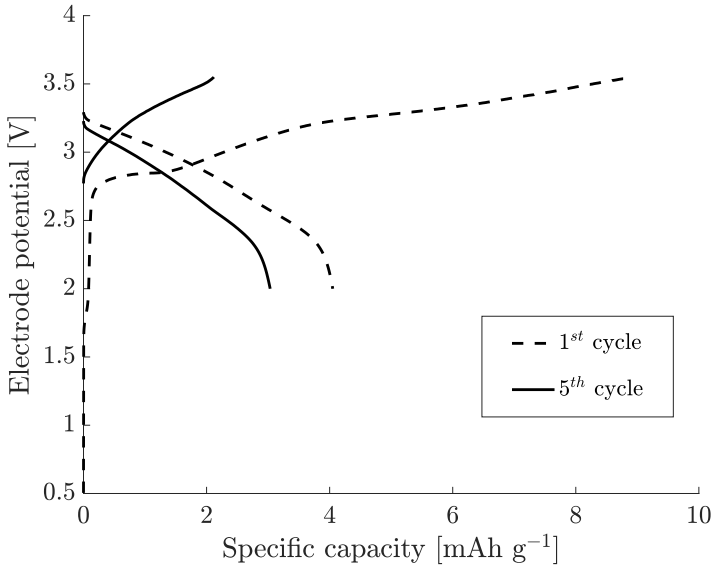

Figure 4.1: The relation between the specific capacity and the electrode potential. The graphs increasing in value represent the lithiation of the cell, while the graphs decreasing in value represent delithiation of the cell.

4.2 Constant state of charge and varying force

The result for the experiment with constant State of Charge (SOC) and varying force has been divided into two sub-chapters, the first for the effect of the strain rate and the other for the effect of state of lithiation.

4.2.1 Effect of strain rate

As mentioned in chapter 3.2.1, two strain rates were used during the experiments, $95 \cdot 10^{-6}$ s^{-1} and $24 \cdot 10^{-5}$ s^{-1}. The figures below, figure 4.2 - 4.4, shows how the potential of each cell changes as the applied load varied over time. For two of the cells, cell A and B, no rest was included in the cycling. While for cell C, a rest of 60 s was included.

For cell A, the potential for the higher rate appears to be slightly more stable than for the lower one, where it increases slightly with each cycle. The potential in figure 4.2 appears also to be stable both before and after the load variation, even the applied force is the same for each cycle.

Cell B was the only one of the three batteries that was charged, this is why it has a slightly higher potential than cell A and C. The results in figure 4.3 shows that the cell was subjected to similar forces during the two experiments, but that the potential is slightly lower for the higher strain rate. It can also be viewed that the potential decreases for each cycle and continues to decrease for the lower strain rate, while for the higher strain rate, the potential decreases for the each cycle but stabilizes afterwards.

The results for cell C shows that the potential is slightly lower for the higher strain rate while subjected to a higher force, which can be studied in figure 4.4. But the relationship between the potential and the force has similar behavior in both graphs. The experiments done for cell C were carried out twice, the second time with a lower rest time, see figure A.1. Similar behavior that can be studied in the graphs for the higher rest time can also be seen in the graphs for the lower one.

The graphs show the same behavior for all cells, regardless of whether they are lithiated or delithiated. It can also be seen that the response to the potential is immediate when the load increases or decreases.

The coupling factor k was calculated using equation (2.4) for each cell and its different strain rates, the results are stated in table 4.1. The values for the coupling factor show a linear elastic behavior, that is, there is no difference as the load increases or decreases.

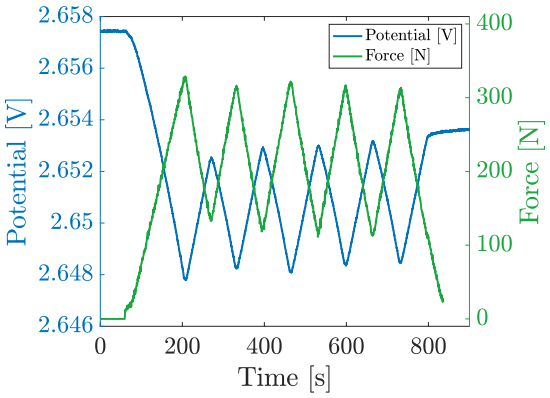

(a) Displacement rate 0.2 mm/min.

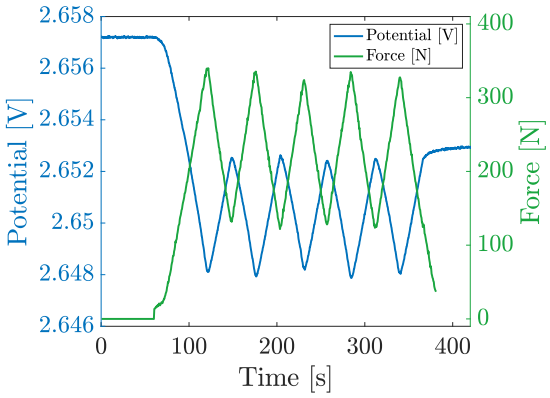

(b) Displacement rate 0.5 mm/min.

Figure 4.2: Potential and corresponding force for cell A with displacement rate 0.2 mm/min and 0.5 mm/min.

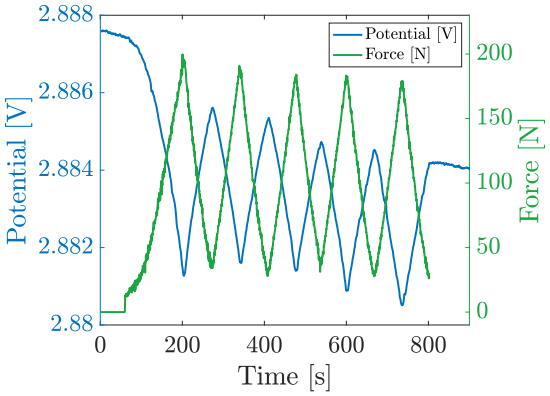

(a) Displacement rate 0.2 mm/min.

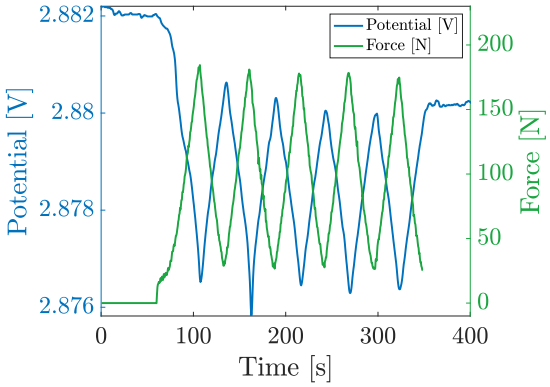

(b) Displacement rate 0.5 mm/min.

Figure 4.3: Potential and corresponding force for cell B with displacement rate 0.2 mm/min and 0.5 mm/min.

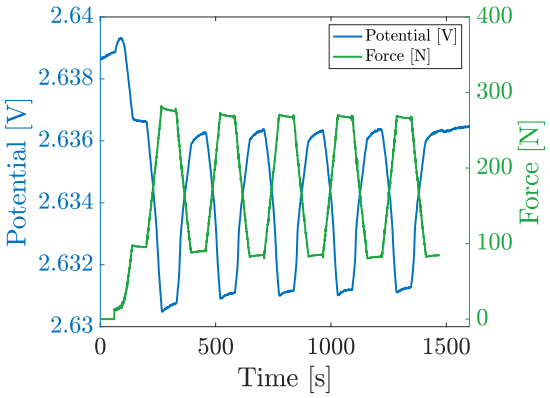

(a) Displacement rate 0.2 mm/min.

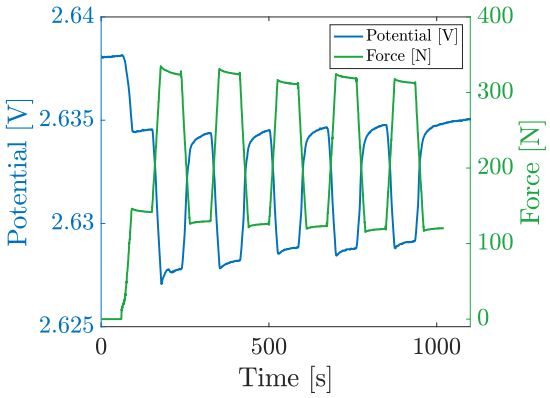

(b) Displacement rate 0.5 mm/min.

Figure 4.4: Potential and corresponding force for cell C with displacement rate 0.2 mm/min and 0.5 mm/min.

Table 4.1: The calculated coupling factor for the different cells and the two different strain rates.

Cell	State of charge [%]	Strain rate $[s^{-1}]$	Increasing force	Decreasing force
A	0	$95 \cdot 10^{-6}$	0.8213	0.8400
		$24 \cdot 10^{-5}$	0.8267	0.8217
B	100	$95 \cdot 10^{-6}$	0.6954	0.6409
		$24 \cdot 10^{-5}$	0.6162	0.6909
C	0	$95 \cdot 10^{-6}$	0.9642	0.9087
		$24 \cdot 10^{-5}$	1.2447	1.0543

4.2.2 Effect of state of lithiation

The results from cell B show no major difference from the results from cell A and cell C, other than that the potential is slightly higher and the load slightly lower for cell B. When studying the coupling factor in table 4.1, it can be seen that the lithiated cell has a lower coupling factor compared to the two delithiated cells.

4.3 Mechanical tests

Figure 4.5 shows the mechanical tests for a lithiated cell and a delithiated cell. The graphs shows that the delithiated cell is subjected to a higher force than the lithiated cell.

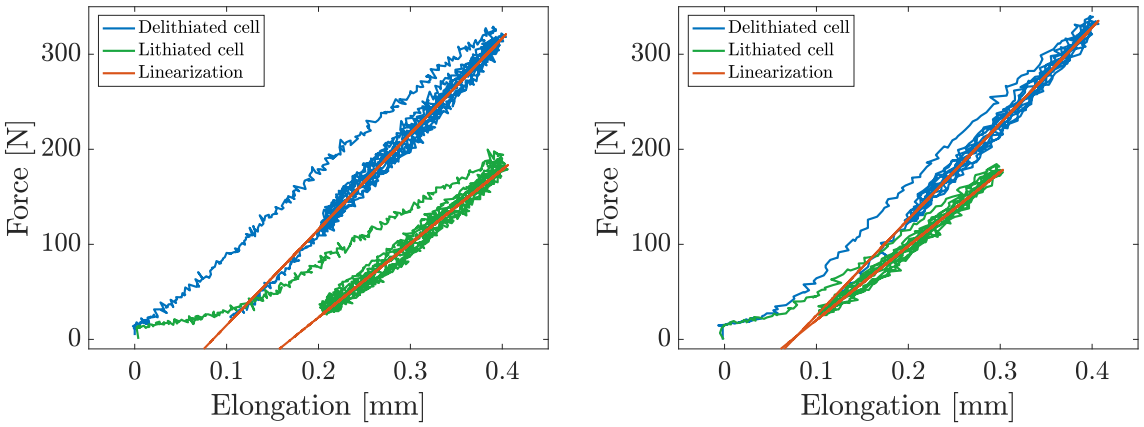

(a) Displacement rate 0.2 mm/min. **(b)** Displacement rate 0.5 mm/min.

Figure 4.5: Mechanical tests of a lithiated cell and a delithiated cell.

5

Discussion

The aim of this thesis was to develop methods for characterization of laminated structural batteries under combined eletrochemical and mechanical loads. The goal was to determine to what extent the potential of the structural battery changes when a constant current and a varying mechanical load is applied.

The model that has been used to perform the experiments already exists but no one has previously attempted to map the coupling factor and its effect on the structural battery.

5.1 Battery performance

In general, structural batteries perform quite poorly in terms of capacity compared to regular Li-ion batteries. This is largely due to inhibited ion transport between the electrodes due to the SBE. The reason the cells show a reduced capacity between the first and fifth cycles is that they are not conditioned, i.e. they have not been cycled very slowly. Such conditioning is usually performed to reach a reversible capacity of the cell.

In a study done by Asp et al. [2] they have produced the voltage profiles for cells with different C-rates, i.e. how fast a cell charges where C rate 1 C corresponds to a fully charged battery in 1 hour. The results show that for a lower C rate a higher specific capacity is obtained than for a higher C rate. In this study, a C rate of 0.1 C has been used. The result from this study is comparable to the result from Asp et al., and this result lies between the result for the cells with a C rate of 0.15 C and 0.05 C. Thus, the cells used in this study show similar behavior to the cells used in the previous study. Based on the comparison with the previous results, it can be concluded that the cells in this study are functioning well. It should be kept in mind is that the results in the previous study are normalized against the active material, i.e. the material responsible for the lithiation. While in this thesis, the SBE, the separator and the aluminum foil have also been included in the calculations and therefore a lower capacity has been measured.

5.2 Simultaneously electrochemical and mechanical testing

The response of the potential when the cell is submitted to a varying load is not strain rate dependent. Although the displacement rates used are very low, and can be seen as quasi-static, it can be concluded that the potential change is not strain rate dependent. However, to validate the results and the conclusion, more experiments need to be conducted with higher displacement rates.

When comparing the results of this thesis with the results of a similar experiment on the half-cell carried out by Jacques et al. [22], it can be determined that the results agree well with each other. The full-cell exhibits the same behavior as the half-cell. What should be kept in mind when comparing these results is that the half-cell is lithiated when the full-cell is delithiated and delithiated when the full-cell is lithiated. This results in that as the load increases, the potential of the half-cell also increases, while the potential of the full-cell decreases as the load increases, and vice versa.

It can be difficult to draw any concrete conclusions as not enough experiments have been carried out in this study. Some trends can be seen, including that for the cell that was fully charged, the coupling factor is lower than for the cells that were fully discharged. In any case, it can be said that the coupling factor is affected by the SOC the cell has.

The similar behavior for the two experiments done on cell C with different rest times shows repeatability in the experiments.

The mechanical tests performed on two of the cells, cell A and B, show similar behavior for both strain rates. The delithiated cell can take a higher load than the non-lithiated cell can. In figure 4.5b, it can be observed that the lithiated cell has an extension between 0.1 mm and 0.3 mm, while the delithiated cell in the same graph has an extension between 0.2 mm and 0.4 mm. This is because the delithiated cell was re-tensioned in the tensile machine after the first experiment with the lower displacement speed and the program was thus reset. However, for the lithiated cell, it was not re-tensioned, but the program was reset and restarted, resulting in where the last program ended became the beginning of the new program. In this case, the cell was already extended 0.1 mm when the program was started, so the cell is thus extended between the same values as before, only that the program assumes it is moving between two new values.

5.3 Piezo-electrochemical effect

The Piezo-electrochemical effect is measured as a linearly response of the OCP to the carbon fiber loaded in tension.

Harnden et al. [23] have done similar experiments as in this study but with half-cells instead of full-cells. The results from that study show that when the cell is completely delithiated, a coupling factor of just over 1 is obtained. The coupling factor then increases in value and the maximum value is reached around 1.5 when the cell has a SOC of about 50 %, then the coupling factor decreases again to a value of about 1.3 when the cell is 100 % lithiated. As the experiments in this study are not as extensive, no maximum value for the coupling factor can be estimated. The conclusions that can be drawn if a comparison with Harnden's results is made, is that the trend for a full-cell is the opposite of that for a half-cell. Using these comparisons, conclusions can be drawn that the results of this study are reasonable. Since the carbon fiber in the half-cell acts as the positive electrode while for the full-cell the carbon fiber acts as the negative electrode, the results should be inverted compared to each other, something that can be seen here.

Although the coupling factor in this study is slightly lower than the result from Harnden's [23], between 1.3 and 1.5 for Harnden's result and 0.8 and 1 for the results in this study, the results are of the same order of magnitude. With this, conclusions can be drawn that the result is within reasonable limits. One reason why the result in this study is somewhat lower may have to do with the fact that only the cell was clamped into the tensile machine, while in Harnden's experiment the cell was clamped into the tensile machine while it was still in the pouch bag. Also, Harnden and co-workers performed tests only on carbon fibers in liquid electrolyte. Since tests reported here are performed in SBE, the difference in the measured coupling factor can also be due to this.

5.4 Implementation challenges

Since no strain gauge could be attached to the cell, due to the size and mechanical performance of the matrix, no accurate reading of the strain could be possible and the results may therefore deviate from the actual results. But if a strain gauge would have been attached to the cell, it would have been attached with glue and there would have been a risk of it measuring the stiffness of the glue instead of the cell because the glue would have a higher stiffness than the matrix.

Of the 24 cells that were produced during the course of the work, only three of these produced results. This was due to several different things, some known and some unknown. One of the known causes was that the SBE did not cure properly and caused the tabs to slide apart when the cell was clamped in the tensile machine and subjected to loads. Another known cause was that the LFP foil detached from the cell, this also happened when the cell was exposed to loads in the tensile

machine. The reason behind why the LFP foil came off is unclear, but one theory could be that the SBE did not cure properly. There were also problems with the tabs sliding apart during the curing process, this resulted in the cell could not be properly clamped in the tensile machine. Some of the cells did not work at all, this was most often detected in the electrochemical cycling. The reason behind it is unknown, but one theory could be a short circuit in the cell.

When the cell was clamped into the tensile machine, it was noted that the potential dropped as the screws were tightened. This was probably due to the cell being subjected to compressive forces in the tabs and thus changing the potential. In this thesis, this has been disregarded, as the interest was in studying the potential when the cell was subjected to tensile loads and not compressive loads. However, it may be good to note that this occurs for future experiments.

As previously mentioned, the potential was affected by the clamping in the tensile machine, this thus resulted in a 3 dimensional load is addition to the applied a tensile load. This may have affected the results, but to what extent has not been established and it is something that may be good to take into account if more similar experiments are to be carried out.

The machine compliances present in the tensile machine were neglected, but noted in these experiments. Values from the second cycle were used to calculate the coupling factor. The second cycle was chosen because during the first cycle the cell is not subjected to a constant tensile load, but during the subsequent cycles it is subjected to a constant tensile load.

5.5 Future research

This thesis successfully demonstrates the coupling between electrical potential and mechanical strain for a structural battery, both in the charged and discharged states. Overall, a significant amount of work remains in terms of both basic research and reaching industrial applications for structural batteries. Specifically, to fully understand and utilize the electrochemical-mechanical coupling effect for strain sensing, why several research activities are proposed here.

Firstly, it should be emphasized that the battery cell design studied in this thesis employs commercial electrode films as the positive electrode. Current research is underway to replace this film with coated carbon fibers as the multifunctional positive electrode. It is of high interest to conduct similar experiments with this all-fiber structural battery to exploit any additional Piezo-electrochemical effects.

The experiments on the Piezo-electrochemical response to the OCP carried out in this thesis should be repeated and extended to establish the coupling effect for different SOC. Furthermore, the coupling factor, which is measurement of the strain sensitivity, should be examined for different electrochemical loadings.

A series of experiments in which the battery cell is subjected to and held under static mechanical load, while a current, either positive or negative, is run through the battery, would allow for the evaluation of the strain sensitivity at different C-rates. Understanding the voltage-strain coupling at high C-rates is of interest for high-power devices.

Experiments that maintain the cell potential constant while applying varying tensile strain to the battery cell at different states of charge would allow for the evaluation of using this multifunctional material for energy harvesting, as a change in current is expected as an immediate response to the applied tension.

Additionally, there are many other mechanical load cases of interest apart from the in-plane tensile load examined in this thesis, such as in-plane compression, shear, and out-of-plane bending.

Finally, the results presented in this thesis can be used to verify and validate modeling results. Experiments are essential to provide input parameters for accurately predicting the multifunctional performance in two-way coupled multiphysics electro-chemo-mechanical models of the structural battery [25]. Improved predictability is not only vital for the development of the structural battery but also of interest to other research fields, such as battery management systems, where the SOC of each battery cell in a battery pack is one of the most critical indicators.

Recently, data-driven methods using statistical and machine learning techniques have gained popularity in the battery research community. The data gathered from experiments can be leveraged to develop a so-called digital twin model, which opens the possibility of estimating device-level performance.

6
Conclusion

The purpose of this thesis was to develop methods for characterization of laminated structural batteries under combined electrochemical and mechanical loads. The goal was to study the change in potential when the structural battery is subjected to a constant SOC and a varying mechanical load.

The results shows that when the mechanical load is increased there is a drop in the potential, and when the cell is unloaded, the potential increases. However, a certain variation can be studied in the potential between the different load cycles. This could possibly have been avoided if a more accurate tensioning of the cell was done in the tensile machine or if it could be said with greater certainty that the SBE cured properly and no slippage occurred during the experiment.

The values for the coupling factor show a linear elastic behavior for all three cells. The result for the coupling factor enables additional functions beyond the structural battery. In order to draw more detailed conclusions, more experiments must be carried out with cells of different SOC.

The experiments carried out in this thesis has never been done before and although the results are good, further work is needed to validate the results. More experiments need to be performed with cells at different SOC. If this is done and the results are similar to those in this thesis, the next step can be taken in the development of structural batteries.

The model used in this study has been used in previous experiments where the half-cell has been studied, but this is the first study of its kind to be carried out on a full-cell. The result shows that the model works for experiments where the full-cell is studied. However, more and more detailed studies need to be carried out to gain a better understanding of the full-cell, the coupling factor and its behavior.

Bibliography

[1] UniEnergy Technologies, "How much does a tesla battery weigh? (ultimate guide)." https://www.uetechnologies.com/how-much-does-a-tesla-battery-weigh/. [Online; Accessed 22-January-2023].

[2] L. E. Asp, K. Bouton, D. Carlstedt, S. Duan, R. Harnden, W. Johannisson, M. Johansen, M. K. G. Johansson, G. Lindbergh, F. Liu, K. Peuvot, L. M. Schneider, J. Xu, and D. Zenkert, "A structural battery and its multifunctional performance," *Advanced Energy and Sustainability Research*, vol. 2, no. 3, p. 2000093, 2021.

[3] D. Carlstedt and L. E. Asp, "Performance analysis framework for structural battery composites in electric vehicles," *Composites Part B: Engineering*, vol. 186, p. 107822, 2020.

[4] L. Asp, M. Johansson, G. Lindbergh, J. Xu, and D. Zenkert, "Structural battery composites: A review," *Functional Composites and Structures*, vol. 1, 11 2019.

[5] UL Research Institute, "What are lithium-ion batteries?." https://ul.org/research/electrochemical-safety/getting-started-electrochemical-safety/what-are-lithium-ion, Sept. 14, 2021.

[6] J. Xu, Z. Geng, M. Johansen, D. Carlstedt, S. Duan, T. Thiringer, F. Liu, and L. E. Asp, "A multicell structural battery composite laminate," *EcoMat*, vol. 4, no. 3, p. e12180, 2022.

[7] J. P. Thomas and M. A. Qidwai, "Mechanical design and performance of composite multifunctional materials," *Acta Materialia*, vol. 52, no. 8, pp. 2155–2164, 2004.

[8] J. Thomas and S. Qidwai, "Mechanical design and performance of composite multifunctional materials," *Acta Materialia*, vol. 52, pp. 2155–2164, 05 2004.

[9] L. E. Asp and E. S. Greenhalgh, "Structural power composites," *Composites Science and Technology*, vol. 101, pp. 41–61, 2014.

[10] C. Meng, N. Muralidharan, E. Teblum, K. Moyer, G. Nessim, and C. Pint, "Multifunctional structural ultra-battery composite," *Nano Letters*, vol. 18, 11 2018.

[11] L. Asp, S. Leijonmarck, T. Carlson, and G. Lindbergh, "Realisation of structural battery composite materials," 07 2015. ICCM 20, Copenhagen, Denmark.

[12] A. Thakur and X. Dong, "Printing with 3d continuous carbon fiber multifunctional composites via uv-assisted coextrusion deposition," *Manufacturing Letters*, vol. 24, 02 2020.

[13] J. M. Pappas, A. R. Thakur, and X. Dong, "Effects of cathode doping on 3d printed continuous carbon fiber structural battery composites by uv-assisted co-extrusion deposition," *Journal of Composite Materials*, vol. 55, no. 26, pp. 3893–3908, 2021.

[14] E. Jacques, M. H. Kjell, D. Zenkert, G. Lindbergh, M. Behm, and M. Willgert, "Impact of electrochemical cycling on the tensile properties of carbon fibres for structural lithium-ion composite batteries," *Composites Science and Technology*, vol. 72, no. 7, pp. 792–798, 2012.

[15] M. Y. Tan, D. Safanama, S. S. Goh, J. Y. C. Lim, C.-H. Lee, J. C. C. Yeo, W. Thitsartarn, M. Srinivasan, and D. W. H. Fam, "Concepts and emerging trends for structural battery electrolytes," *Chemistry – An Asian Journal*, vol. 17, no. 21, p. e202200784, 2022.

[16] J. Xu, W. Johannisson, M. Johansen, F. Liu, D. Zenkert, G. Lindbergh, and L. E. Asp, "Characterization of the adhesive properties between structural battery electrolytes and carbon fibers," *Composites Science and Technology*, vol. 188, p. 107962, 2020.

[17] L. E. Asp, "Multifunctional composite materials for energy storage in structural load paths," *Plastics, Rubber and Composites*, vol. 42, no. 4, pp. 144–149, 2013.

[18] L. B. B. Agarwal and K. Chandrashekhara, *Analysis and performance of fiber composites*. John Wiley and Sons Inc, 4th ed. ed., 2018.

[19] S. Duan, A. H. Iyer, D. Carlstedt, F. Rittweger, A. Sharits, C. Maddox, K.-R. Riemschneider, D. Mollenhauer, M. Colliander, F. Liu, and L. E. Asp, "Effect of lithiation on the elastic moduli of carbon fibres," *Carbon*, vol. 185, pp. 234–241, 2021.

[20] UN Academy, "Structure of graphite and uses." `https://unacademy.com/content/jee/study-material/chemistry/structure-of-graphite-and-uses/`, 2023. [Online; accessed 4-May-2023].

[21] D. Hull and T. W. Clyne, *Fibres and matrices*, p. 9–38. Cambridge Solid State Science Series, Cambridge University Press, 2 ed., 1996.

[22] E. Jacques, M. H. Kjell, D. Zenkert, and G. Lindbergh, "Piezo-electrochemical effect in lithium-intercalated carbon fibres," *Electrochemistry Communications*, vol. 35, pp. 65–67, 2013.

[23] R. Harnden, D. Zenkert, and G. Lindbergh, "Potassium-insertion in polyacrylonitrile-based carbon fibres for multifunctional energy storage, morphing, and strain-sensing," *Carbon*, vol. 171, pp. 671–680, 2021.

[24] R. Harnden, K. Peovot, D. Zenkert, and G. Lindbergh, "Multifunctional performance of sodiated carbon fibers," *Electrochemical Society*, vol. 165, pp. 616–622, 2018.

[25] D. Carlstedt, K. Runesson, F. Larsson, J. Xu, and L. E. Asp, "Electro-chemo-mechanically coupled computational modelling of structural batteries," *Multifunctional Materials*, vol. 3, p. 045002, 2020.

A

Appendix 1

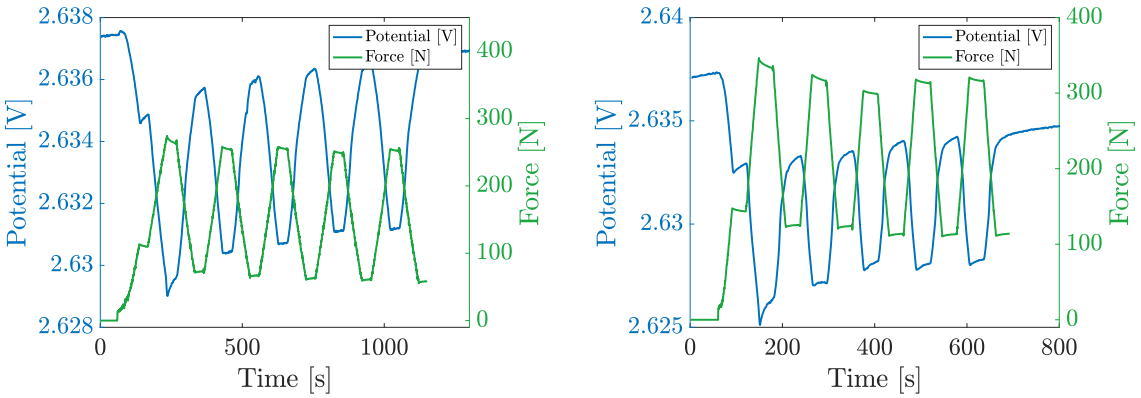

(a) Displacement rate 0.2 mm/min.

(b) Displacement rate 0.5 mm/min.

Figure A.1: Potential and corresponding force for cell C with displacement rate 0.2 mm/min and 0.5 mm/min with a rest of 30 s.

DEPARTMENT OF SOME SUBJECT OR TECHNOLOGY
CHALMERS UNIVERSITY OF TECHNOLOGY
Gothenburg, Sweden
www.chalmers.se

CHALMERS
UNIVERSITY OF TECHNOLOGY